Journal of Materials Chemistry

Cite this: J. Mater. Chem., 2011, 21, 9290

www.rsc.org/materials

PAPER

Growth mechanism of $Ni_{0.3}Mn_{0.7}CO_3$ precursor for high capacity Li-ion battery cathodes

Dapeng Wang,[ab] Ilias Belharouak,*[a] Gary M. Koenig, Jr,[a] Guangwen Zhou[b] and Khalil Amine[a]

Received 11th March 2011, Accepted 15th April 2011
DOI: 10.1039/c1jm11077b

Transition metal carbonate ($Ni_{0.3}Mn_{0.7}CO_3$) was co-precipitated as the precursor for Li- and Mn-enriched composite materials used as advanced cathodes for lithium-ion batteries. The optimal pH range for synthesis of $Ni_{0.3}Mn_{0.7}CO_3$ in a continuous stirred tank reactor (CSTR) at the pilot scale was predicted by taking into account the chemical equilibriums between the products and reactants. The nucleation and growth of precursor particles were investigated during the CSTR process by monitoring particle size distributions, particle morphologies, chemical compositions, and structures with time. It was found that in the early stage of co-precipitation both the particle size distribution and the chemical composition were not homogeneous; a lead time of about 5 hours under our experiment conditions was necessary to achieve the uniformity in particle shape and chemical composition. The latter was not altered during extended times of co-precipitation; however, a continuous growth of particles resulted in relatively large particles (D_{50} > 30 μm). The electrochemical performance of the final lithiated cathode materials is reported.

Introduction

Composite lithium- and manganese-rich $Li_{1+x}M_{1-x}O_2$ compounds (M = Mn, Ni, Co) have become attractive cathode materials because of their high capacity (>200 mA h g^{-1}) and enhanced structural stability.[1–6] The electrochemical performance of these materials strongly depends upon the physical properties of the precursor materials that serve as sources for lithiation.[7–9] In current Li-ion battery materials, hydroxide co-precipitation is largely used to produce transition metal hydroxide precursors.[5,10,11] This method, however, is problematic for producing precursors with high manganese content because Mn^{2+} can easily be oxidized to Mn^{3+}, forming manganese oxy-hydroxide (MnOOH) and leading to a deviation from the desired stoichiometry. Also, the resulting Mn-rich hydroxide precursors often have irregular morphology and low packing density, which result in low energy density and unsuitable electrochemical performance. Carbonate co-precipitation has, therefore, emerged as an alternative method to produce transition metal (Mn, Ni, Co) precursors.[12–15] The main advantage is that in the carbonate matrix, the oxidation state of the cations is kept as 2+ for all transition metals. Also, the experimental conditions under which carbonates are usually made are less harsh than those of the hydroxide process, namely, the pH value is usually close to 8 as opposed to 11. Co-precipitation in the continuous stirred tank reactor (CSTR) has been widely used in the synthesis of small quantities of carbonate precursors due to its advantages such as homogeneous composition, narrow particle size distribution, high tap density, and facile scale-up to the few hundreds of grams collected over a short time.[12–15] However, no comprehensive study is available in the literature on the carbonate particle growth as a function of CSTR reaction time. The present research gives insights into the nucleation and growth mechanism of carbonate precursors prepared by the CSTR co-precipitation process in large production output. Our goal was to determine the CSTR experimental conditions that influenced the chemical homogeneity, morphology, and physical properties of carbonate precursors (and, subsequently, the electrochemical characteristics of the final materials) during production.

Material and methods

Nickel sulfate hexahydrate ($NiSO_4 \cdot 6H_2O$), manganese sulfate monohydrate ($MnSO_4 \cdot H_2O$), sodium carbonate (Na_2CO_3), and ammonium hydroxide ($NH_3 \cdot H_2O$) were used as the starting materials to prepare $Ni_{0.3}Mn_{0.7}CO_3$ precursor. A schematic of the water-jacketed CSTR system is shown in Fig. 1. First, 2 M sodium carbonate and 0.2 M ammonium hydroxide were dissolved in de-ionized water in feeding tank #1. Then, nickel and manganese sulfates were dissolved in de-ionized water in feeding tank #2 to prepare a 2 M transition metal solution with a Mn/Ni atomic ratio fixed at 7/3. The two feeding tanks were connected to peristaltic pumps. Solution in tank #1 was connected to a pH controller set at 8.3 in a contact mode. Solution in tank #2 was pumped in at a feeding rate of about 1 L h^{-1}. The reaction

[a]Chemical Sciences and Engineering Division, Argonne National Laboratory, 9700 South Cass Avenue, Argonne, IL, 60439, USA. E-mail: belharouak@anl.gov; Tel: +1 630-252-4450
[b]Department of Mechanical Engineering, State University of New York at Binghamton, Binghamton, NY, 13902, USA

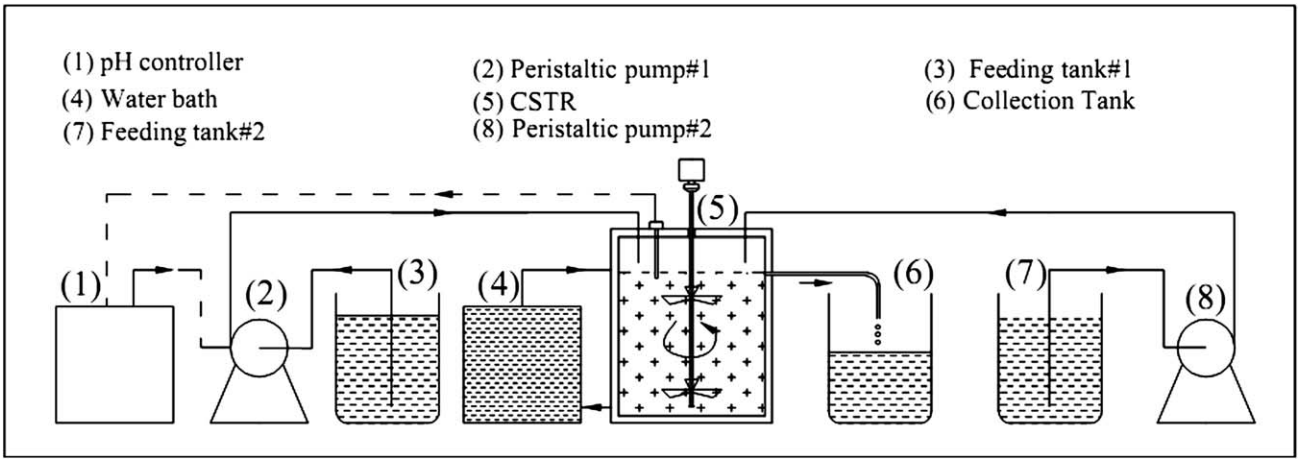

Fig. 1 Schematic drawing of CSTR system used for this experiment.

temperature was controlled at 52 °C. Product overflow was periodically collected during the experiment, and the particle size distribution was measured with a particle size analyzer (Cilas 1090). The precursor material, which was used to prepare the cathode materials, was collected from hour 5 to hour 8 of the process. Collected samples were washed with hot water several times to remove residual sodium and sulfuric species, then filtered and dried inside a vacuum oven set at 100 °C over 24 hours.

The morphologies of the particles were characterized by cold field emission scanning electron microscopy (FE-SEM, Hitachi S-4700-II). Energy dispersive X-ray spectrometry (EDXS) was used to qualitatively determine the Mn/Ni atomic ratio of the collected particles. The average composition of the samples was determined by EDXS from dozens of particles. X-Ray powder diffraction (XRD) patterns were recorded with a D5000 Siemens X-ray diffractometer, using a Cu-Kα radiation source (λ = 1.5406 Å). The samples were scanned from 5 to 80° at a scan rate of 20 s per 0.02°.

The cathode material $Li_{1.5}(Ni_{0.3}Mn_{0.7})O_{2+\gamma}$ was prepared from appropriate amounts of $Ni_{0.3}Mn_{0.7}CO_3$ and Li_2CO_3, where γ was 0.45 based on a valence balance (Li^+, Ni^{2+}, Mn^{4+} and O^{2-}). The mixture was calcined at 900 °C for 15 hours. The electrochemical properties of $Li_{1.5}(Ni_{0.3}Mn_{0.7})O_{2+\gamma}$ were evaluated in tests using CR-2032 type cells. The cathode was made of 80% active material, 10% acetylene black, and 10% polyvinylidene difluoride (PVDF) binder coated onto aluminium foil. Cells were assembled inside a helium-filled glove box with lithium metal as the counter anode. A Celgard 2325 membrane was use as the electrode separator. The electrolyte was 1.2 M $LiPF_6$ dissolved in ethylene carbonate (EC) and ethyl methyl carbonate (EMC) (3 : 7 vol% ratio). The cells were tested in the voltage range of 2.0–4.6 V at a constant current density of 20 mA g^{-1} at room temperature.

Results and discussion

In a CSTR, the production of homogeneous and stoichiometric precursor particles highly depends on the pH of the solution during the co-precipitation of transition metal hydroxides or carbonates. The pH conditions should be well controlled to produce desired precursor materials which have a significant impact on the performance of final materials when mass produced. Bommel and Dahn[16] conducted research to optimize the pH conditions based on the concentration and reaction rate during hydroxide precipitation. Calculations of pH ranges for other co-precipitation systems have also been reported.[17,18] In this research, a theoretical calculation was performed to predict the residual transition metal concentrations in solution during the carbonate co-precipitation process. The calculations were based on the equilibrium reactions shown in Table 1. The value of n in the complex formation equilibriums ranges from 1 to 6 ligands. In addition, M^{2+} ions and $[M(NH_3)_n]^{2-}$ complexes were considered as the residual species in the solution (M = Ni or Mn). A minimum residual transition metal concentration in solution is necessary to produce stoichiometric precursor with the transition metal ratio close to that of the reactants.

Fig. 2 shows the calculated residual Ni and Mn concentration as a function of pH. Four pH zones were established based on the dominant reactions occurring in the solution. When the pH is below 7.5 and above the pH of the initial transition metal solution (zone 1), the carbonate co-precipitation process dominates the CSTR reaction. However, the residual concentrations of Mn and Ni are high in the solution, which would result in precursor with undesired chemical stoichiometry and atomic efficiency. The pH zone between 8.5 and 9.8 (zone 3) has an increase of the residual nickel concentration due to the formation of stable complexes $[Ni(NH_3)_n]^{2-}$ which will distort the stoichiometry of

Table 1 Equilibrium reactions and constants used in calculation of the residual transition metals in the solution

Equilibrium reactions	Equilibrium constant K
$H_2CO_3 \leftrightarrow H^+ + HCO_3^-$	4.3×10^{-7}
$HCO_3 \leftrightarrow H^+ + CO_3^{2-}$	5.62×10^{-11}
$MnCO_3 \leftrightarrow Mn^{2+} + CO_3^{2-}$	2.34×10^{-11}
$NiCO_3 \leftrightarrow Ni^{2+} + CO_3^{2-}$	1.42×10^{-7}
$Mn^{2+} + nNH_3 \leftrightarrow [Mn(NH_3)_n]^{2+}$	See ref 16
$Ni^{2+} + nNH_3 \leftrightarrow [Ni(NH_3)_n]^{2+}$	See ref.16
$Mn(OH)_2 \leftrightarrow Mn^{2+} + 2OH^-$	1.9×10^{-13}
$Ni(OH)_2 \leftrightarrow Ni^{2+} + 2OH^-$	5.48×10^{-16}
$NH_3 \cdot H_2O \leftrightarrow NH_4 + OH^-$	5.7×10^{-10}
$H_2O \leftrightarrow OH^- + H^+$	10^{-14}

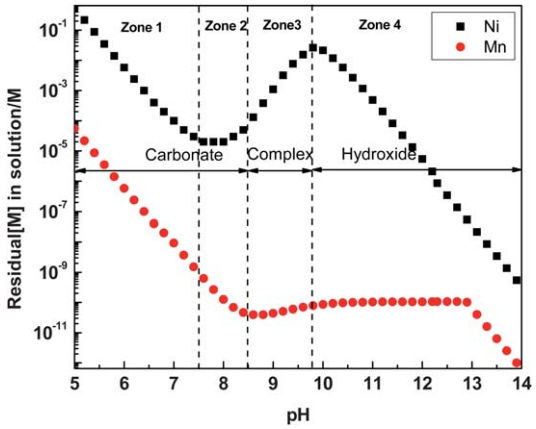

Fig. 2 Predicted residual transition metal concentration in solution as a function of pH.

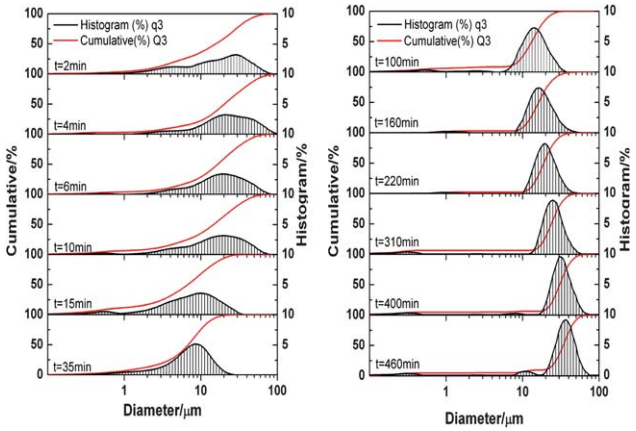

Fig. 3 Particle size distribution of samples collected at different reaction times.

the co-precipitated particles. When the pH is above 9.8 (zone 4), the hydroxide co-precipitation process will dominate the overall CSTR reaction. In this case, the decrease of the residual Ni concentration is mostly due to the formation of nickel hydroxide, which is not a desired product for the carbonate co-precipitation process described here. In the pH zone 7.5–8.5 (zone 2), the competition between the carbonate co-precipitation reaction and the ammonia complex formation minimizes the residual concentration of the transition metals in solution, which provides the best reaction conditions to attain the desired stoichiometry of $Ni_{0.3}Mn_{0.7}CO_3$. A pH value of 8.3 was selected for the co-precipitation of $Ni_{0.3}Mn_{0.7}CO_3$ carbonate.

Co-precipitation using a CSTR is a complex process. Besides the complexity of the chemical reactions and kinetics, several other factors such as feeding rate, concentration of the acidic and basic solutions, stirring rate, reactor volume, and impeller and baffle shapes are important to the nucleation and growth of particles and, therefore, to the morphology of the final precursor. In some instances, models were used to predict the seeding and growth mechanism of particles in CSTR reaction;[19–21] however, when some of the important factors listed above were changed, the models had to be modified accordingly. The nucleation can change from heterogeneous primary or secondary nucleation to homogeneous nucleation, and the driving force for the growth may shift between diffusion controlled and surface integration controlled.[22,23] Instead, we experimentally monitored the nucleation and growth processes by analyzing the particle size distribution (Fig. 3 and 4), morphology (Fig. 5), composition (Fig. 6), and structures (Fig. 7) as a function of the reaction time. The structure and morphology (Fig. 8) and electrochemical performance (Fig. 9 and 10) of the final cathode material were also analyzed.

Fig. 3 shows the particle size distribution of particles collected during the 8 hours of CSTR co-precipitation. At the very beginning (first 2 minutes), the particle distribution was unexpectedly broad, with particle sizes ranging from 1 to 80 μm. We speculated the large particles were formed by agglomeration of very small seeds (Fig. 5). The agglomeration is likely due to the electrostatic force or surface tension between the seed particles. As time elapses (up to 10 min), the particle size distribution narrowed slightly, and the distribution maximum shifted to a center around 20 μm. In addition, a small peak appeared below 1 μm, possibly due to the disintegration of the large agglomerates (Fig. 3). After 15 min, the curve became a single distribution peak, with the maximum increasing to 8 μm (35 min), 14 μm (100 min), 16 μm (160 min), and up to 36 μm at the end of the CSTR experiment.

Fig. 4 shows the evolution of the average particle size (D50) with time. During the first 35 min of the reaction, D50 decreased from 20 to 8 μm, in agreement with the data in Fig. 3. Thereafter, D50 increased almost linearly during the rest of the experiment. The calculated growth rate of the average diameter was 3.4 μm per hour. During the collection time (Fig. 3), the average size of the particles increased from 24 μm (300 min) to 34 μm (460 min). As a result, the individual particles grew in mass, even though the feeding rate was kept constant during the co-precipitation. The possible explanation is that some additional nucleation sites were available at the surface of the freshly formed particles for further growth.

Fig. 5 shows SEM images of the precursors collected during the CSTR experiment. The SEM images were chosen to reflect the trend of particle nucleation and growth during the co-precipitation process. During the first minutes (2 min) of the experiment, the precursor particles were composed of large loose agglomerates with no defined shape. Thereafter, some spherical agglomerates were formed with different sizes. After 35 min, more segregation was observed within the agglomerations, and

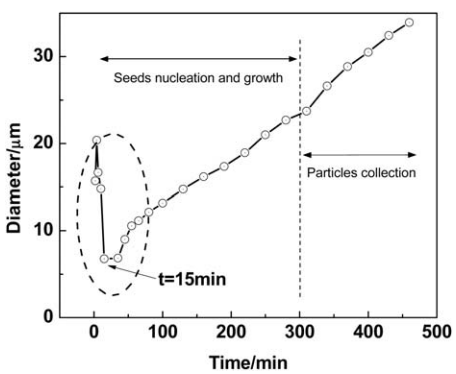

Fig. 4 Average particle size (D50) evolution as a function of time.

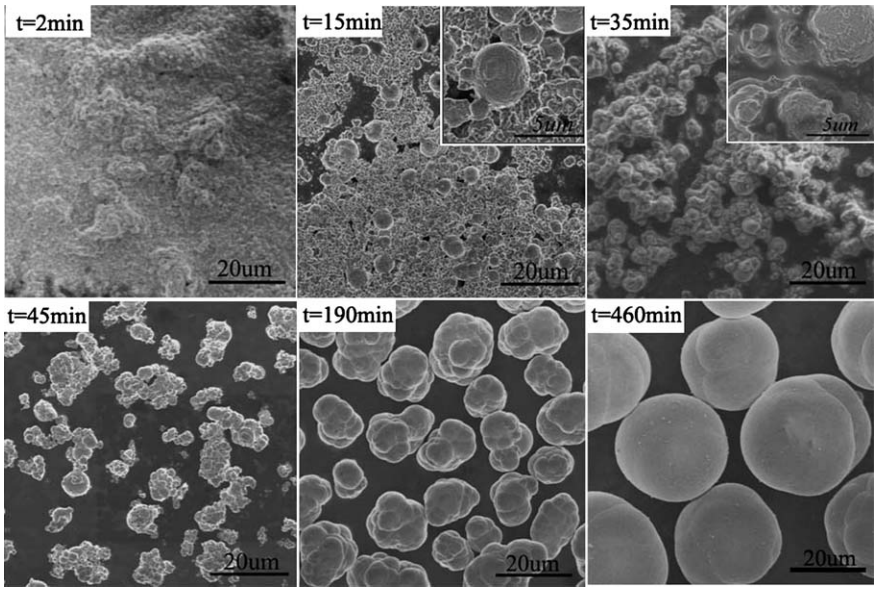

Fig. 5 SEM images of samples collected at different reaction times.

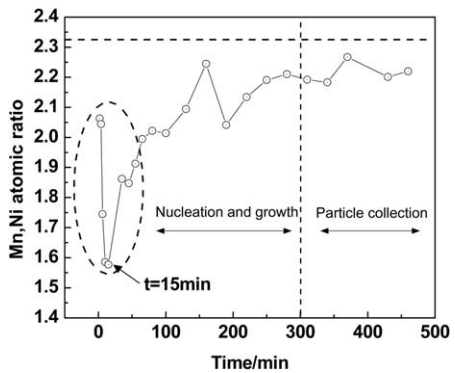

Fig. 6 EDXS of samples collected at different reaction times.

particles continued to grow with a round shape. These SEM observations were in accordance with the particle size distribution results detailed in Fig. 3 and 4. The surface of the final collected particle was apparently smooth and dense; however,

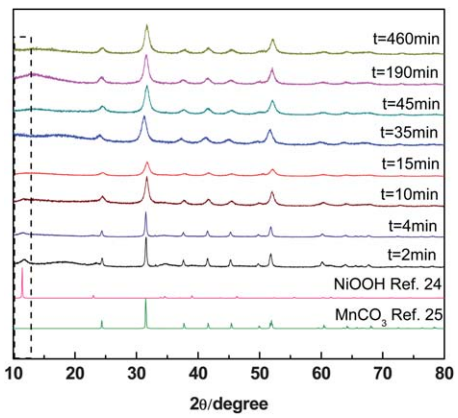

Fig. 7 X-Ray diffraction patterns of samples from different collection times.

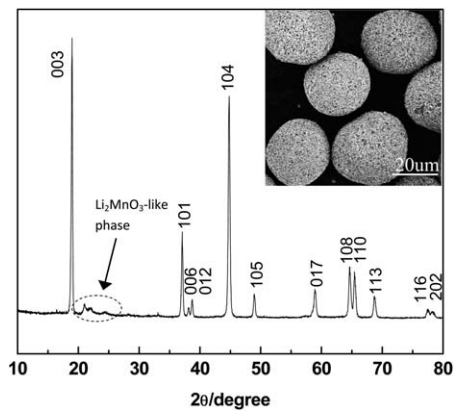

Fig. 8 X-Ray diffraction patterns of $Li_{1.5}(Ni_{0.3}Mn_{0.7})O_{2+\gamma}$. Inset is SEM image.

a surface analysis performed by the BET method showed that these particles had a large surface area of 152 $m^2\ g^{-1}$ with an average pore size of 1.7 nm. Therefore, we concluded that these

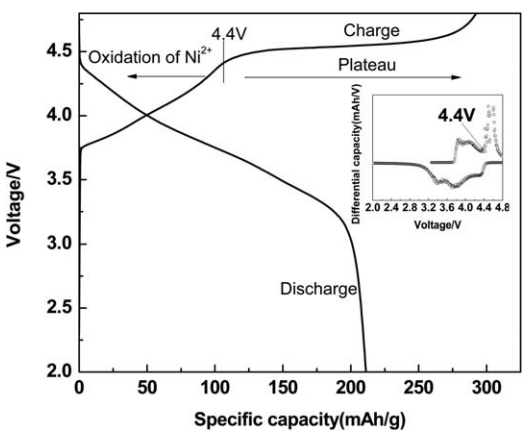

Fig. 9 The first charge–discharge profile of $Li_{1.5}(Ni_{0.3}Mn_{0.7})O_{2+\gamma}$.

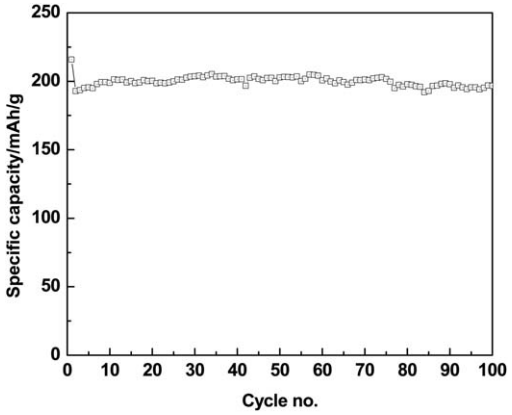

Fig. 10 Cycling performance of $Li_{1.5}(Ni_{0.3}Mn_{0.7})O_{2+\gamma}$ under 20 mA g^{-1} current density and voltage window 2–4.6 V.

spherical precursor particles were actually secondary particles composed of nano-size primary particles of the same chemical composition.

Fig. 6 shows the compositions measured using EDXS obtained on particles collected during the co-precipitation reaction. Our qualitative analysis of the transition metals showed that the Mn/Ni atomic ratio fluctuated with time early in the process and then became more stable after 5 hours of reaction. The horizontal dotted line in Fig. 6 shows the nominal Mn/Ni atomic ratio expected under our experimental conditions. A huge deviation of the nominal and measured Mn/Ni atomic ratio was apparent at the beginning of the co-precipitation reaction (Fig. 4). As time increased, the Mn/Ni atomic ratio increased and then approached the desired ratio after 5 hours of co-precipitation. For this reason, the precursor particles that were selected for the electrochemical study were collected after 5 hours of co-precipitation.

X-Ray diffraction provided further structure and phase information of the samples collected during the nucleation and growth processes (Fig. 7). It can be seen that the main component of the precipitates was carbonates; however, at an early stage, the small broad peak at $2\theta = 11.6°$ was consistent with the formation of nickel oxyhydroxide impurity.[24] This peak became less important for the subsequent sample and finally disappeared after 15 min. At the beginning of the co-precipitation, NiOOH formed because it is thermodynamically much more stable than $NiCO_3$ and also because the possibly localized high pH value within the reactor favors the formation of the hydroxide. At the early stage of the reaction a competition between the hydroxide and carbonate co-precipitation may have occurred because of the likelihood of fluctuations in pH and transition metal concentration inside the reactor. The peak signature of the observed nickel oxyhydroxide was very broad possibly due to the nano-character of the co-precipitated phase, in agreement with the SEM image of Fig. 5 at $t = 2$ min. Thereafter, as the solution became more homogeneous, the pH in the CSTR reactor stabilized, and therefore, the carbonate co-precipitation process dominated the reaction and gave rise to the production of spherical carbonate precursor particles (Fig. 5 and 7).[25] Since the particles formed before 5 hours were less homogeneous in chemical composition and morphology, they were not used as the precursor for the preparation of the cathode material.

The precursor particles, which were collected during hours 5–8 of the co-precipitation process and used to prepare the cathode material, had XRD pattern consistent with manganese carbonate, although the peaks were relatively broad (Fig. 7), which is likely due to the small grain size of the precursor particles. After lithiation, the cathode material $Li_{1.5}(Ni_{0.3}Mn_{0.7})O_{2+\gamma}$ had a surface area of only 1 m^2 g^{-1} because during the high temperature calcination with lithium carbonate, the nano-primary particles fused to one another, resulting in larger primary particles without change in the morphology of the secondary particles (Fig. 8). The structure of $Li_{1.5}(Ni_{0.3}Mn_{0.7})O_{2+\gamma}$ was primarily indexed based on the $R\bar{3}m$ space group, which is the structure of the major layered component in similar materials, with the existence of a secondary component belonging to the Li_2MnO_3-like phase.[11,26–29]

The first charge and discharge profile of $Li_{1.5}(Ni_{0.3}Mn_{0.7})O_{2+\gamma}$ in a CR-2032 lithium cell is shown in Fig. 9. The current density was 20 mA g^{-1}, which was equivalent to C/10 assuming that 200 mA g^{-1} is achieved at the 1 C rate. The cell was initially charged to 4.8 V, discharged to 2 V, and then cycled between 2 and 4.6 V in the subsequent cycles. During the first charge, the initial capacity (110 mA h g^{-1}) observed below 4.4 V is due to the oxidation of Ni^{2+} to Ni^{4+}, and the capacity (182 mA h g^{-1}) observed in the plateau region between 4.4 and 4.8 V is correlated with the activation of Li_2MnO_3, in agreement with previous reports.[12,30,31] The first discharge capacity was 210 mA h g^{-1} with the first cycle columbic efficiency of 72%. Fig. 10 shows the cycling behavior of the $Li_{1.5}(Ni_{0.3}Mn_{0.7})O_{2+\gamma}$ in a lithium cell under the C/10 rate. As can be seen, starting from the second cycle, the discharge capacity of 200 mA h g^{-1} was retained for over 100 cycles. The large particles (~30 μm) possibly limited the lithium diffusion and led to electrochemically inactivated core. Further processing and optimization of the co-precipitation parameters to produce precursor particles less than 20 μm can improve the capacity of the $Li_{1.5}(Ni_{0.3}Mn_{0.7})O_{2+\gamma}$ material.

Conclusions

A CSTR was used to synthesize $Ni_{0.3}Mn_{0.7}CO_3$, and the nucleation and growth of the precursor particles were monitored as a function of time. The pH zone that favors carbonate co-precipitation reaction was calculated based on the thermodynamic equilibrium between the chemical species existing in the reaction medium. Particle size analysis combined with SEM, EDX, and XRD results confirmed that the nucleation and growth process began with the formation of a mixture composed of a carbonate-type dominating phase and a nickel oxyhydroxide-type impurity phase, which disappeared with time. The co-precipitation reaction started with the formation of seed particles having irregular shape and fluctuating chemical stoichiometry, and ended with the production of spherical, homogeneous particles of carbonate precursor with a chemical composition close to the nominal one. These precursor particles continued their growth during the 8 hours of CSTR reaction and reached a final average diameter of 35 μm. This trend was also observed for different experimental conditions, indicating that the continued particle growth is typical for producing transition metal carbonates. Future work will focus on addressing this phenomenon so that the spherical precursor particles could be

mass produced with smaller average size (around 15–20 μm). These properties along with better chemical homogeneity would help in the acceptance of this carbonate co-precipitation process as an alternative route to the well-established hydroxide process by industries working in the production of precursors for cathode materials in lithium-ion batteries.

Acknowledgements

This research was funded by the U.S. Department of Energy, Freedom CAR, and Vehicle Technologies Office. The electron microscopy analysis was accomplished at the Electron Microscopy Center for Materials Research at Argonne National Laboratory, a U.S. Department of Energy Office of Science Laboratory operated under Contract No. DE-AC02-06CH11357 by UChicago Argonne, LLC.

References

1 J.-H. Kim, C. S. Yoon and Y.-K. Sun, *J. Electrochem. Soc.*, 2003, **150**, A538.
2 Z. Lu and J. R. Dahn, *J. Electrochem. Soc.*, 2002, **149**, A815.
3 C. S. Johnson, J.-S. Kim, C. Lefief, N. Li, J. T. Vaughey and M. M. Thackeray, et al., *Electrochem. Commun.*, 2004, **6**, 1085–1091.
4 S. H. Kang, Y. K. Sun and K. Amine, *Electrochem. Solid-State Lett.*, 2003, **6**, A183.
5 Z. Lu, D. D. MacNeil and J. R. Dahn, *Electrochem. Solid-State Lett.*, 2001, **4**, A191.
6 T. A. Arunkumar, E. Alvarez and A. Manthiram, *J. Electrochem. Soc.*, 2007, **154**(8), A770–A775.
7 K. Lee, S. Myung, J. Moon and Y. Sun, *Electrochim. Acta*, 2008, **53**, 6033.
8 H. Bang, B. Park, J. Prakash and Y. Sun, *J. Power Sources*, 2007, **174**, 565.
9 G. Kim, S. Myung, H. Kim and Y. Sun, *Electrochim. Acta*, 2006, **51**, 2447.
10 C. S. Johnson, J.-S. Kim, A. J. Kropf, A. J. Kahaian, J. T. Vaughey, L. M. L. Fransson, K. Edström and M. M. Thackeray, *Chem. Mater.*, 2003, **15**, 2313–2322.
11 M. M. Thackeray, S.-H. Kang, C. S. Johnson, J. T. Vaughey and S. A. Hackney, *Electrochem. Commun.*, 2006, **8**, 1531–1538.
12 D.-K. Lee, S.-H. Park, K. Amine, H. J. Bang, J. Parakash and Y.-K. Sun, *J. Power Sources*, 2006, **162**, 1346–1350.
13 K.-S. Lee, S.-T. Myung, H. J. Bang, S. Chung and Y.-K. Sun, *Electrochim. Acta*, 2007, **52**, 5201–5206.
14 J.-H. Lim, H. Bang, K.-S. Lee, K. Amine and Y.-K. Sun, *J. Power Sources*, 2009, **189**, 571–575.
15 S.-H. Park, S.-H. Kang, I. Belharouak, Y. K. Sun and K. Amine, *J. Power Sources*, 2008, **177**, 177–183.
16 A. van Bommel and J. R. Dahn, *Chem. Mater.*, 2009, **21**, 1500–1503.
17 D. H. Chen, S. R. Sheen, C. T. Chang, C. Y. Shei and W.-M. Hurng, *J. Mater. Res.*, 1992, **7**, 2317–2323.
18 L. Marta, et al., *Science*, 2003, **2**, 72–82.
19 A. Mersmann and M. Kind, *Chem. Eng. Technol.*, 1988, **11**, 264–276.
20 R. Zauner and A. G. Jones, *Chem. Eng. Sci.*, 2000, **55**, 4219–4232.
21 I. H. Leubner, *Curr. Opin. Colloid Interface Sci.*, 2000, **5**, 151–159.
22 O. Sohne and J. W. Mullin, *J. Cryst. Growth*, 1978, **44**, 377–382.
23 N. S. Tavare, *AIChE J.*, 1995, **41**, 2537–2548.
24 O. Glemser and J. Einerhand, *Z. Anorg. Allg. Chem.*, 1950, **261**, 43–51.
25 H. Effenberger, K. Mereiter and J. Zemann, *Z. Kristallogr.*, 1981, **156**, 233–243.
26 M. M. Thackeray, C. S. Johnson and J. T. Vaughey, *J. Mater. Chem.*, 2005, **15**, 2257–2267.
27 A. D. Robertson and P. G. Bruce, *Chem. Mater.*, 2003, **15**, 1984–1992.
28 S.-H. Kang, S.-H. Park, C. S. Johnson and K. Amine, *J. Electrochem. Soc.*, 2007, **154**, A268–A274.
29 I. Belharouak, G. M. Koenig, Jr, J. Ma, D. P. Wang and K. Amine, *Electrochem. Commun.*, 2011, **13**, 232–236.
30 A. Robert Armstrong, M. Holzapfel and P. Novak, *J. Am. Chem. Soc.*, 2006, **128**, 8694–8698.
31 J.-H. Lim, H. Bang and K.-S. Lee, *J. Power Sources*, 2009, **189**, 571–575.